International Journal of Pharmaceutics 670 (2025) 125109

Contents lists available at ScienceDirect

International Journal of Pharmaceutics

journal homepage: www.elsevier.com/locate/ijpharm

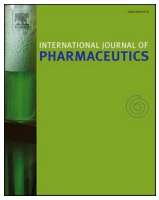

Incorporation of ionizable lipids into the outer shell of lipid-coated calcium phosphate nanoparticles boosts cellular mRNA delivery

Masoomeh Khalifeh [a], Rik Oude Egberink [a], Rona Roverts [a], Roland Brock [a,b,*]

[a] Department of Medical BioSciences, Radboud University Medical Center, The Netherlands
[b] Department of Medical Biochemistry, College of Medicine and Medical Sciences, Arabian Gulf University, Manama 329, Bahrain

ARTICLE INFO

Keywords:
Calcium phosphate nanoparticle
Endosomal escape
mRNA
Ionizable lipid
Nanomedicine

ABSTRACT

Messenger RNA is a highly promising biotherapeutic modality with great potential in preventive and therapeutic vaccination, and in the modulation of cellular function through transient expression of therapeutic proteins. However, for cellular delivery, mRNA requires packaging into delivery vehicles that mediate uptake and also shield the mRNA against degradation. Lipid-coated calcium phosphate (LCP) nanoparticles encapsulate the mRNA in a calcium phosphate core, which is coated by a bilayer of structural lipids, positively charged lipids and pegylated lipid to mediate cellular uptake and achieve colloidal stabilization. Here, we show that such nanoparticles using positively charged lipids achieve cellular uptake but only poor cytosolic mRNA delivery. However, mRNA release could be greatly enhanced through incorporation of ionizable lipids into the outer leaflet of the lipid bilayer. We optimized the composition and molar ratios of ionizable lipids, positive lipid, cholesterol, and polyethylene glycol (PEG) and evaluated the potency of the formulations for the cellular delivery of mRNA. Whereas in lipid nanoparticles, the ionizable lipid has a main role in the complexation of the mRNA, our study provides a new paradigm for the employment of ionizable cationic lipids in nanocarriers other than lipid nanoparticles (LNPs) to boost the endosomal release of nucleic acids.

1. Introduction

RNA-based therapies, which either act through providing therapeutic proteins to cells by mRNA delivery or through siRNA-mediated gene silencing, offer new treatment options for various diseases (Dunbar et al., 2018; Pardi et al., 2018; Sahin et al., 2014). The delivery of mRNA to produce therapeutic proteins has several potential benefits compared to the delivery of DNA or proteins. For mRNA, there is no need for nuclear entry, thus it also works in non-dividing, differentiated cells and proteins will have all naturally occurring posttranslational modifications. However, there are significant obstacles to RNA therapy including instability due to rapid degradation by nucleases and the size and negative charge of RNA that limit its cellular uptake. Therefore, considerable efforts have been directed towards the development of delivery systems to overcome these limitations (Hajj and Whitehead, 2017; Hou et al., 2021). Currently, non-viral lipid-based vectors are the most frequently used vectors, which exhibit promising properties in protecting the mRNA cargo from RNase digestion and facilitating cellular uptake by endocytosis and endosomal release. Endosomal escape is one of the key challenges for exploiting the therapeutic activity of RNAs (Schlich et al., 2021). Several strategies have been pursued to promote endosomal escape, as for example, the incorporation of protonatable groups to induce a proton-sponge effect (Vermeulen et al., 2018), the use of lipids that form non-lamellar phases (Zuhorn et al., 2005), and the decoration of the vector surface with cationic, membrane-active peptides (Hatakeyama et al., 2009). For lipid nanoparticles, pH-dependent ionizable lipids do not only play a role in the complexation of RNA but also trigger release by forming inverted hexagonal phase non-bilayer structures at low pH that destabilize the endosomal membrane (Paloncýová et al., 2021).

Recently, lipid-coated calcium phosphate (LCP) nanoparticles (NPs) have been developed that consist of a core-membrane structure that can be loaded with a variety of materials such as nucleic acids, chemotherapeutics and radionucleids (Movahedi et al., 2021; Satterlee et al.,

Abbreviations: DLS, Dynamic Light Scattering; DOPA, Di-oleoyl-phosphatidic acid; DOPC, 1,2-dioleoyl-*sn*-glycero-3-phosphocholine; DOTAP, di-oleoyl-trimethylammonium propane; DSPE-PEG 2000, 1,2-distearoyl-*sn*-glycero-3-phosphoethanolamine-N-[amino(polyethylene glycol)-2000]; LCP, lipid-coated calcium phosphate; LNPs, Lipid Nanoparticles; NPs, Nanoparticles; SecNLuc, Secreted Nano-Luciferase; SD, standard deviation; TEM, Transmission Electron Microscopy.

* Corresponding author at: Dept. of Medical BioSciences, Radboud University Medical Center, Geert Grooteplein 28, 6525 GA, Nijmegen, The Netherlands.
E-mail address: roland.brock@radboudumc.nl (R. Brock).

https://doi.org/10.1016/j.ijpharm.2024.125109
Received 19 September 2024; Received in revised form 17 December 2024; Accepted 18 December 2024
Available online 19 December 2024

2015; Tang et al., 2015; Wang et al., 2018; Yang et al., 2012). Nucleic acid cargoes can be readily co-precipitated in the LCP core, which provides compaction and protection. The calcium phosphate core is then encapsulated into a lipid bilayer which is formed in a two-step layer-by-layer process thereby enabling asymmetry in the lipid layer composition. Although LCPs were initially established for intravenous delivery of siRNA, they have also been explored for the delivery of mRNA (Wang et al., 2018). In LCP NPs, the calcium phosphate core is acid-sensitive and can dissolve in the endosome, promoting endosomal escape for intracellular nucleic acid delivery (Li et al., 2010). By comparison, so far, no membrane-active components were included in the lipid bilayer which so far consisted out of a positively charged lipid such as di-oleoyl-trimethylammonium propane (DOTAP), cholesterol, structural lipid and pegylated lipid. In the present study, we incorporated the ionizable lipids DLin-DMA (Jayaraman et al., 2012), ALC-0315 (Hope et al., 2017), and SM-102 (Benenato et al., 2017), into the outer leaflet of the LCP NPs. Whereas in this case, the ionizable lipids do not play a role in the complexation of the RNA we were curious to learn whether they would still enhance endosomal release.

We formulated the ionizable lipid based LCP NPs (iLCP) by combination of ionizable lipids with different molar fractions of DOTAP, cholesterol, and polyethylene glycol (PEG). All formulations were characterized with respect to hydrodynamic diameter and zeta potential, transfection efficiency, and toxicity. Overall, incorporation of ionizable lipids into the outer leaflet of the LCP NPs greatly enhanced cellular uptake and mRNA delivery.

2. Materials and methods

2.1. Materials

Polyoxyethylene (5) nonylphenylether (IGEPAL CO-520) and cholesterol were purchased from Sigma Aldrich. Di-oleoyl-phosphatidic acid (DOPA), 1,2-distearoyl-*sn*-glycero-3-phosphoethanolamine-N-[amino(polyethylene glycol)-2000], (DSPE-PEG 2000), 1,2-dioleoyl-*sn*-glycero-3-phosphocholine (DOPC), and DOTAP were from Avanti Polar Lipids, and the ionizable lipids DLin-DMA, SM-102 and ALC-0315 from Broadpharm (San Diego, CA, USA). Messenger RNA coding for Secreted Nano-Luciferase (SecNLuc) and AlexaFluor647-labeled eGFP mRNA were purchased from RIBOPRO (Oss, The Netherlands).

2.2. Preparation of LCP nanoparticles

The mRNA-loaded LCP NPs were synthesized using a water-in-oil reverse microemulsion process (Li et al., 2012). In brief, 60 μL $CaCl_2$ (2.5 M) with mRNA (5 μg) and Na_2HPO_4 (12.5 mM, 60 μL, pH > 9) were dispersed in two separate cyclohexane/IGEPAL CO-520 (71:29 V/V, 2 mL) solutions, named calcium phase and phosphate phase, respectively. The two oil phases were allowed to stir for 5 min using magnetic stirrers before mixing the phases, and then 40 μL (20 mM) DOPA in chloroform was added to the combined emulsion and the mixture was stirred for 20 min at room temperature. Next, an equal volume of absolute ethanol was added to the mixture to disrupt the microemulsion. Precipitated mRNA-loaded LCP cores were collected by centrifugation at 10,000 x g for 20 min and were washed twice with ethanol to remove any residual cyclohexane and surfactant. The collected CaP cores were dispersed in 200 μL of chloroform. The final LCP NPs were produced by adding a mixture of outer leaflet lipids containing cholesterol (20 mM), DOTAP (20 mM), and various types of ionizable lipids (DLin-DMA (20 mM), SM-102, and ALC-0315 (50 mM) dissolved in ethanol) in different molar ratios. The chloroform was evaporated and the lipid film was hydrated in water, followed by gentle ultrasound treatment to get well-dispersed LCP NPs. The particle size and zeta potential of LCP NPs were measured in water by dynamic light scattering (DLS; Zetasizer, Nano-ZS, Malvern, UK).

2.3. Electron microscopy

Transmission electron microscopy (TEM) was used to determine the structure of LCP NPs. TEM samples were prepared by adding 5 μL of freshly prepared nanoparticle solution onto a 200-mesh carbon-coated copper grid (Electron Microscopy Sciences). The grids were air-dried for 15–30 min at room temperature. Images were acquired with a JEM-1400Flash (Jeol Ltd., Tokyo, Japan) equipped with a Matataki Flash sCMOS camera (Jeol Ltd., Tokyo, Japan) and LaB6 filament operated at 120 kV.

2.4. Cell culture

The osteoblastic cell line MC3T3-E1 (subclone 4, CRL-2593) was obtained from the American Type Culture Collection (Manassas, VA, USA). Cells were grown in Minimal Essential Medium α (Gibco, USA) containing 10 % fetal calf serum (Gibco, USA) and 100 U/mL penicillin, and 100 μg/mL streptomycin (Sigma-Aldrich) in a 37 °C, humidified incubator containing 5 % CO_2.

2.5. Cellular uptake of mRNA-loaded LCP nanoparticles

Cellular trafficking of LCP NPs was evaluated by confocal microscopy. MC3T3 cells were seeded onto 8-well μ-slides (ibidi, Gräfelfing, Germany) at a density of 10,000 cells/cm^2 and allowed to grow for 24 h. Cells were then transfected with different LCP formulations loaded with AlexaFluor647-labeled mRNA. After 4 h, the transfection medium was removed and phenol red-free Opti-MEM (Gibco, USA) was added for image acquisition. For colocalization experiments, endosomal/lysosomal compartments were stained with LysoTracker red (50 nM; Invitrogen, USA) for 30 min before imaging. After washing twice in PBS, imaging was performed using a Leica TCS SP8 SMD confocal microscope (Leica Microsystems, Mannheim, Germany). The images were processed and quantified using ImageJ (version 1.53f51).

2.6. Protein expression

MC3T3 cells were cultured in 96 well plates (Greiner Bio-One, Kremsmünster, Austria) at a density of 10,000 cells/well and incubated overnight. The next day, cells were transfected with three concentrations of LCP formulations loaded with SecNLuc mRNA in serum-containing medium. After 4 h of transfection, the medium was replaced with fresh medium and cells were incubated for a further 24 h.

Luciferase activity was quantified by the Nano-Glo Luciferase Assay System (Promega) as described by the manufacturer's standard protocol. Briefly, 50 μL of luciferase assay substrate was added to 50 μL of medium from each well in a black 96-well plate (Corning, New York, NY, USA). Following 3 min incubation in the dark, the luminescence was measured using a VICTOR X3 Multilabel Plate Reader (Perkin Elmer, Waltham, MA, USA). Luminescence was corrected for background signal using untreated cells. For assessment of luciferase activity at different time points, 50 μL of media was taken from each well and frozen until measurement, and 50 μL of complete media was added to wells to keep the volume at 100 μL and samples were taken every 24 h up to 96 h.

2.7. Cytotoxicity

MC3T3 cells were seeded at a density of 10,000 cells/well into a 96 well plate under the same assay conditions and transfected with different LCP formulations. After 24 h incubation, 10 μl of 5 mg/ml MTT reagent was added to each well and the plate was incubated for another 4 h at 37°C. Subsequently, the media were removed from the cells and 100 μl of DMSO was added to dissolve the formazan crystals. The absorbance was measured at a wavelength of 570 nm using a microplate reader (Bio-Rad).

2.8. Statistical analysis

Data are presented as mean ± SD (standard deviation) and were analyzed in GraphPad Prism software v.8.0. Statistical significances were determined using one- or two-way ANOVA (analysis of variances) or non-parametric Kruskal-Wallis test. A p value < 0.05 was considered significant and is represented as *, $p < 0.05$; **, $p < 0.01$; ***, $p < 0.001$, ****, $p < 0.0001$.

3. Results and discussion

3.1. In vitro delivery of mRNA with DOTAP-based LCP formulations

Previously, LCP NPs have shown activity in the encapsulation and delivery of mRNA into cells in the context of vaccination (Wang et al., 2018). Therefore, in the present study, we first aimed to deliver mRNA to MC3T3 cells, an osteoblastic cell line, using LCP NPs, and compare expression levels to other vehicles for mRNA delivery. MC3T3 cells are a relevant model in the context of bone regeneration. Moreover, with their spread-out morphology these cells are very suited for the analysis of nanoparticle uptake and trafficking by confocal microscopy. In order to assess cellular uptake, AlexaFluor647-labeled mRNA was formulated with LCP NPs containing DOTAP: cholesterol 1:1, DESP-PEG 2000 (15 %) and cells were analyzed by confocal microscopy after 4 h incubation with these LCP NP. Cells showed uptake as concluded from punctate fluorescence inside cells (Fig. 1A). To assess protein expression, LCP NP were also formulated with eGFP mRNA and mRNA encoding for secreted nano-luciferase. For eGFP, no expression could be detected (Fig. 1B). By comparison, for nano-luciferase expression was observed in a dose-dependent manner (Fig. 1C). However, from our experience we could tell, that expression was relatively inefficient, indicating room for improvement in the mRNA LCP formulations of previous reports (Lin et al., 2022; Wang et al., 2018). Studies on lipid nanoparticles (LNPs) demonstrated that the mRNA payload has an impact on loading and LNP structure (Li et al., 2022). However, in most cases poor endosomal escape of mRNA molecules is the main bottleneck of delivery. In order to identify whether endosomal escape was also limiting for the LCP NP we made use of a protocol recently developed by our laboratory in which the formulation in question is co-incubated with a formulation with proven activity If uptake occurs via the same route (Oude Egberink et al., 2024), then the active formulation will also cause the endosomal release of the less active/inactive formulation and thereby enhance protein expression. When LCP NPs containing SecNLuc mRNA were co-incubated with NPs formed with the cell-penetrating peptide PF14 (Ezzat et al., 2011) and eGFP mRNA, the expression of luciferase increased, compared with cells treated with SecNLuc mRNA-loaded LCPs alone, pointing towards endosomal release as the critical bottleneck (Fig. 1D).

3.2. The use of ionizable lipid in LCP formulations to increase expression efficiency

In lipid nanoparticles, ionizable lipids serve the dual purpose of mRNA complexation and membrane destabilization upon endosomal acidification. This activity is achieved through the positive charge and the conical shape of the lipids (Han et al., 2021). Whereas in LCP NP mRNA complexation is accomplished in the calcium phosphate core, we were curious to explore whether the ionizable lipid would still exert its

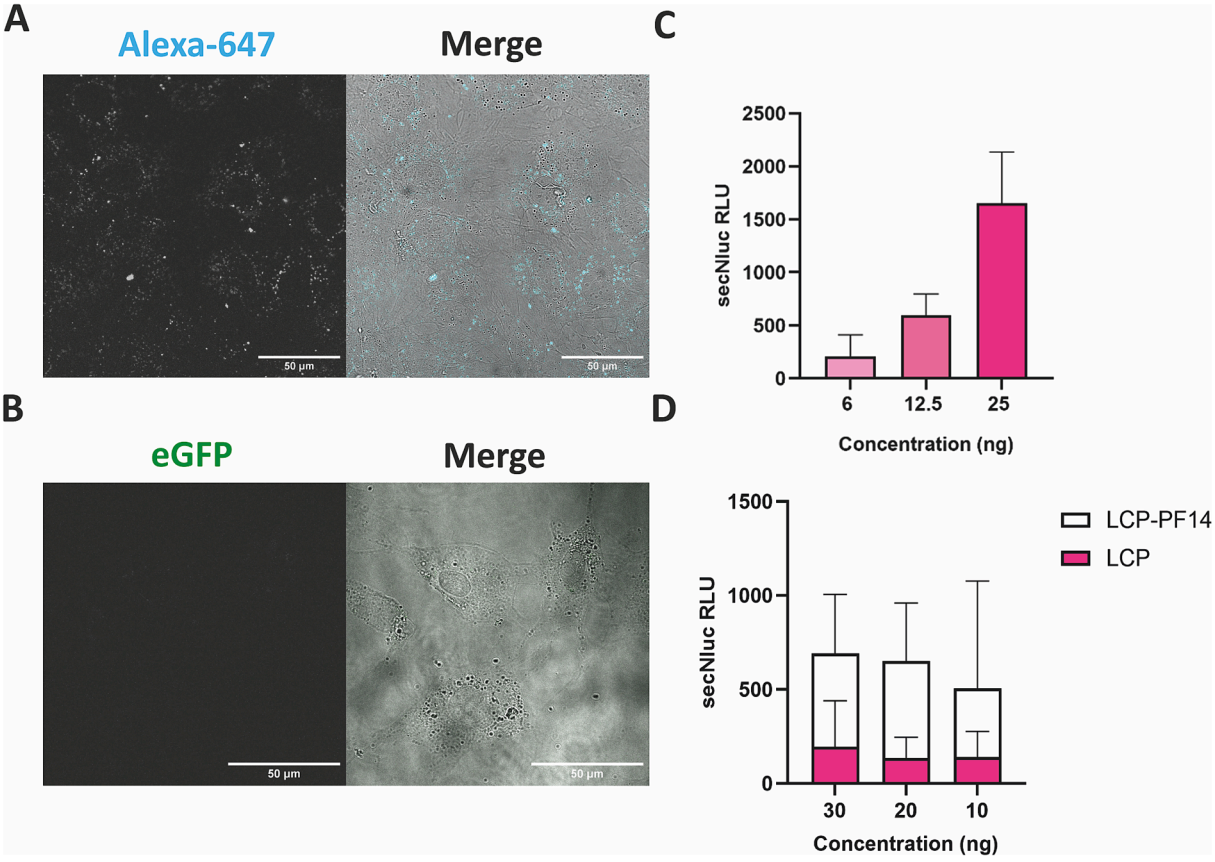

Fig. 1. Cellular delivery of mRNA by LCP NPs. (A) AlexaFluor647-labeled mRNA was formulated in LCPs containing DOTAP, cholesterol, DSPE-PEG 2000, with molar ratio of 42.5/ 42.5/ 15. MC3T3 cells were incubated with LCPs for 4 h and then the images were taken by confocal microscopy. (B) Gene expression activity of LCP NPs in MC3T3 cells transfected with eGFP mRNA. (C) Gene expression activity of LCP NPs in MC3T3 cells transfected with three concentrations of SecNLuc mRNA. (D) Co-transfection of SecNLuc mRNA loaded LCPs with eGFP-PF14 NPs in three dilutions (n = 4).

membrane destabilizing effect when incorporated into the outer leaflet of the lipid bilayer. LCPs were prepared with the ionizable lipids SM-102, ALC-0315, and DLin-DMA. SM-102 (lipid H) and ALC-0315 are the ionizable lipids used by Moderna and Pfizer/BioNTech in their respective SARS-CoV-2 mRNA vaccines (Hou et al., 2021). Both lipids are structurally similar in that two acyl moieties are directly linked to the protonatable tertiary amine and contain either one (SM-102) or two (ALC-0315) branched acyl chains to enhance the conical structure. By comparison DLin-DMA is a first generation ionizable lipid, which is an ether analog of DODAP comprising two unsaturated linoleic acyl chains (Fig. 2A) (Jayaraman et al., 2012).

iLCP NP were prepared with ionizable lipids formulated with DOTAP and cholesterol with a molar ratio of 45:5:50 in the outer layer. In LNPs, the ionizable lipid also comprises about 50 % of the total lipids. A formulation incorporating the neutral lipid DOPC instead of a protonatable lipid was used as control. Luciferase expression was evaluated 24 h after LCP treatment. Incorporation of ionizable lipids into the outer layer yielded significantly higher quantities of SecNLuc protein compared to LCPs without ionizable lipids (Fig. 2B). However, luciferase expression decreased with iLCP concentration suggesting cytotoxicity of the NPs which was confirmed by an in vitro cytotoxicity assay (Fig. 2C). Positive net charge and small size of NPs as well as non-complexed lipids all can exert a cytotoxic effect by interrupting the lipid bilayer (Fröhlich, 2012; Lechanteur et al., 2016; Shang et al., 2014). However, in our case viability was maintained for the DOPC-based LCP NPs. Therefore, the observed toxicity was obviously not related to the charge of the DOTAP cationic lipid. Considering the higher luciferase expression for the iLCP NPs, the data indicates that the ionizable lipids in the iLCP NPs in the present formulations exerted a strong membrane disrupting effect not only inside endosomes but also at neutral pH on the cell surface.

3.3. Optimization of iLCPs to increase expression and decrease cytotoxicity

In order to reduce the cytotoxicity and still maintain activity, we systematically varied the lipid composition of the outer layer. For this step, DLin-DMA was chosen as the ionizable lipid. Seven formulations (coded A through G, Table 1) were created and tested for protein expression and cytotoxicity. Starting with formulations that either only contained the cationic DOTAP lipid (formulation A) or protonatable lipid at different ratios (formulations B, C) next to the structural lipid DOPC and cholesterol, combinations of DOTAP and ionizable lipid (formulations D, E) and finally formulations that additionally incorporated also the pegylated lipid DSPE-PEG2000 in the presence (formulation F) and absence (formulation G) of the cationic lipid were tested. In general, a reduction in ionizable lipid decreased cytotoxicity (Fig. 3B), however, activity was only observed for those formulations that contained 20 mol % of DLin-DMA (Fig. 3A). Absence of toxicity in combination with delivery activity was achieved for the formulation that contained ionizable lipid in combination with DOTAP and pegylation demonstrating that PEG protected the plasma membrane against the membrane activity of the ionizable lipid but still allowed the lipid to exert its activity once inside the endosome. For LNPs it was

Table 1
Lipid compositions and molar ratios of formulations coded A-G.

Formulation	Composition
A	DOTAP/ DOPC/ cholesterol = 10/ 45/ 45
B	DLin-DMA/ DOPC/ cholesterol = 10/ 45/ 45
C	DLin-DMA/ DOPC/ cholesterol = 20/ 40/ 40
D	DOTAP/ DLin-DMA/ DOPC/ cholesterol = 10/ 10/ 40/ 40
E	DOTAP/ DLin-DMA/ DOPC/ cholesterol = 10/ 20/ 30/ 40
F	DOTAP/ DLin-DMA/ cholesterol/ DSPE-PEG2000 = 20/ 20/ 40/ 20
G	DOPC/ DLin-DMA/ cholesterol/ DSPE-PEG2000 = 20/ 20/ 40/ 20

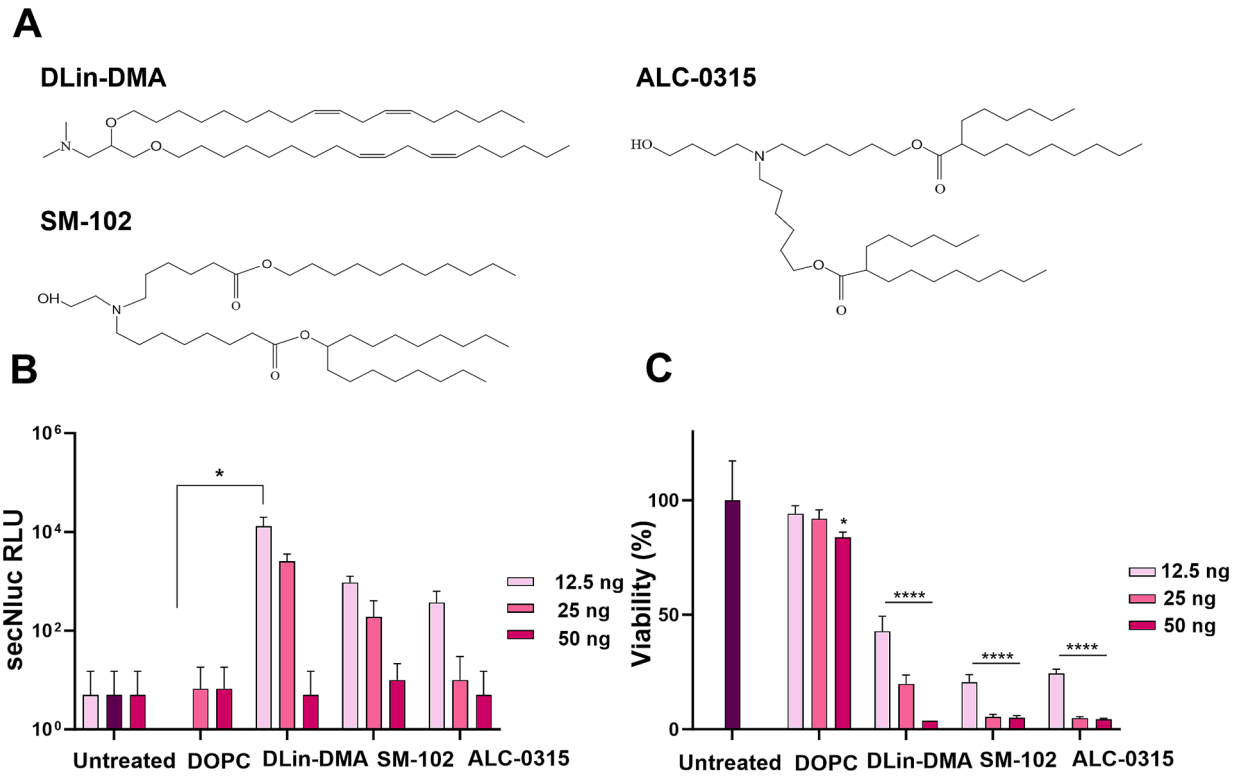

Fig. 2. In vitro transfection efficiency and toxicity of LCP formulations containing DLin-DMA, SM-102, and ALC-0315 as ionizable lipids. (A) Chemical structure of tested ionizable lipids. (B) Luciferase activity in MC3T3 cells transfected with iLCPs for 24 h (n = 4). (C) Cell viability following transfection with iLCPs for 24 h (n = 4). Data are shown as mean ± SD and P < 0.05 was considered statistically significant.

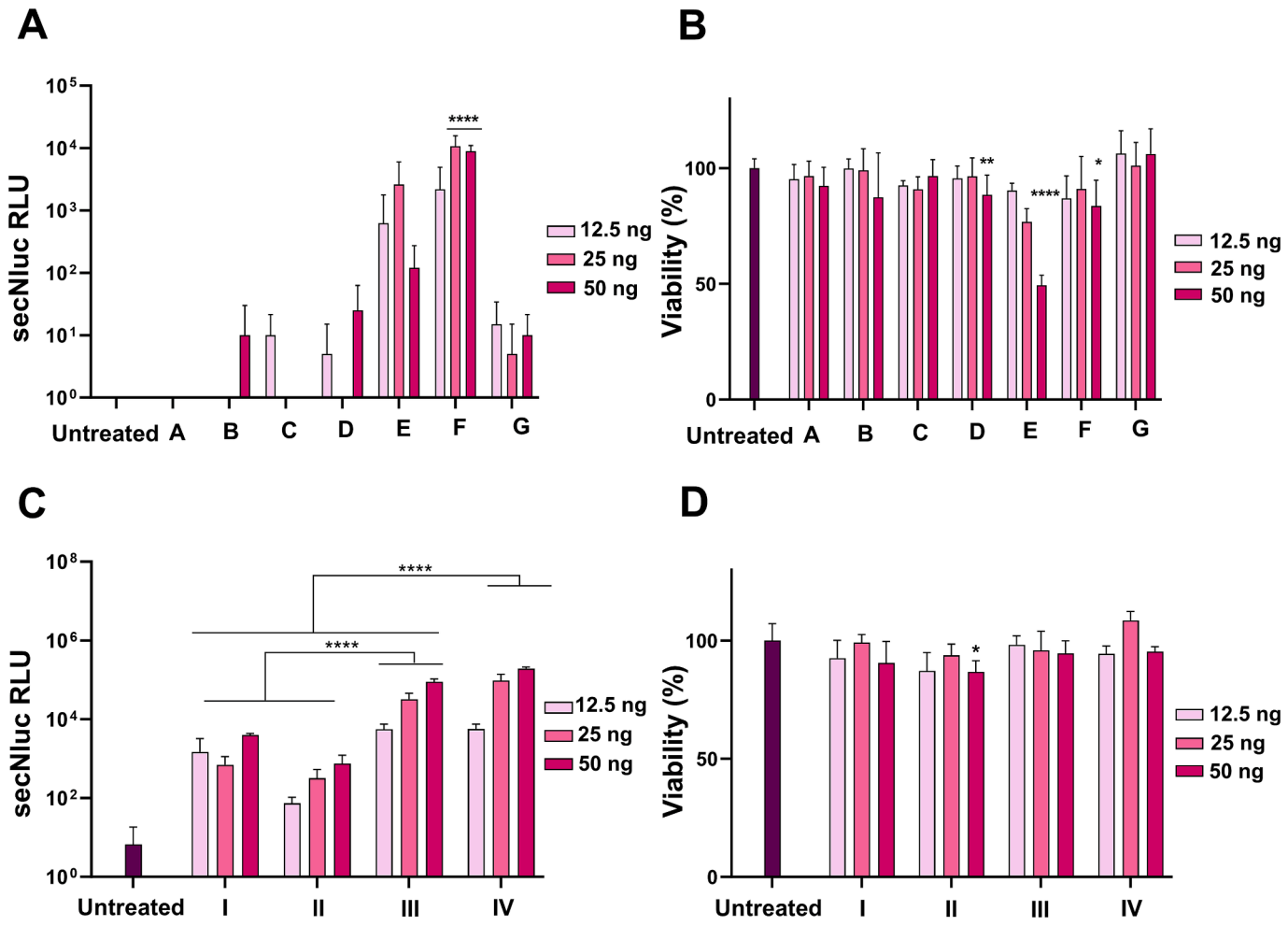

Fig. 3. Optimization of iLCPs formulations. (A, B) Relative luciferase expression and cell viability of MC3T3 cells 24 h after incubation with iLCP formulations coded A-G, differing in lipid components (n = 4, Table 1). (C, D) Relative luciferase expression and cell viability of MC3T3 cells after 24 h transfected with formulations coded I – IV which had a similar lipid composition as formulation F with variation of molar ratios of the individual components (n = 3, Table 2). Data are shown as mean ± SD and $P < 0.05$ was considered statistically significant.

demonstrated that disruption of the endosomal membrane upon fusion of the lipid NP into the lipid bilayer is associated with a transition of the lipids from lamellar to inverted hexagonal (Lα-HII) phase (Ramezanpour and Tieleman, 2022). However, steric hinderance produced by PEG layer around the lipoplexes can disrupt the organization of the lipids in the hexagonal phase (Rabanel et al., 2014). In the endosomes, pH-dependent protonation could release the ionizable lipid from the iLCP NP through charge repulsion. PEGylation can furthermore reduce toxicity by decreasing the surface charge of cationic NPs.

To further optimize the active formulation F, four formulations (I-IV) with DLin-DMA, DOTAP, cholesterol, and DSPE-PEG 2000 at different molar ratios were generated with formulation F of the previous set corresponding to formulation I in this set (Table 2). Given the shielding effect of the pegylated lipid, we increased the mole fraction of the ionizable lipid at the expense of either DOTAP (formulation II) or cholesterol (formulations III and IV). Formulations III and IV yielded the highest activities with approximately ~ 90,000 and 200,000 RUL, respectively (Fig. 3C). Importantly, for formulations II – IV there was a clear dose dependence of activity, and no toxicity at any concentration (Fig. 3D).

A combination of higher concentrations of both DOTAP and the ionizable lipid yielded the highest activity. Many studies detected a significant positive correlation between surface charge and gene transfection efficiency of NPs (Albanese et al., 2012). Yu et al. showed that a higher gene silencing potency was achieved by combination of permanently and ionized cationic lipids in the LNP formulation (Yu et al., 2014). Importantly, however, this higher activity was only observed if at the same time also PEG was included. It is interesting to note that the PEG did not compromise the cellular uptake mediated by the DOTAP lipid.

Table 2
Molar ratios of the lipid compositions in formulations coded I-IV.

formulation	Molar ratio of lipids (DOTAP/DLin-DMA/Cholesterol/ DSPE-PEG2000)
I	20 /20 / 40/ 20
II	10/ 30/ 40/ 20
III	25/ 25/ 30/ 20
IV	20/ 30/ 30/ 20

3.4. LCP formulation based on different ionizable lipids

After optimization of the LCP formulation for DLin-DMA, we then investigated the efficacy of mRNA delivery with the three different ionizable lipids using the same mole fractions of the individual lipids. Strong luciferase expression was observed for all ionizable lipids; however, ALC-0315 containing iLCP NPs were ten times more active than DLin-DMA-containing iLCP NPs, and SM-102-containing iLCP NPs even one hundred times more active (Fig. 4A). These results are also consistent with other studies in which SM-102-containing LNPs exhibited

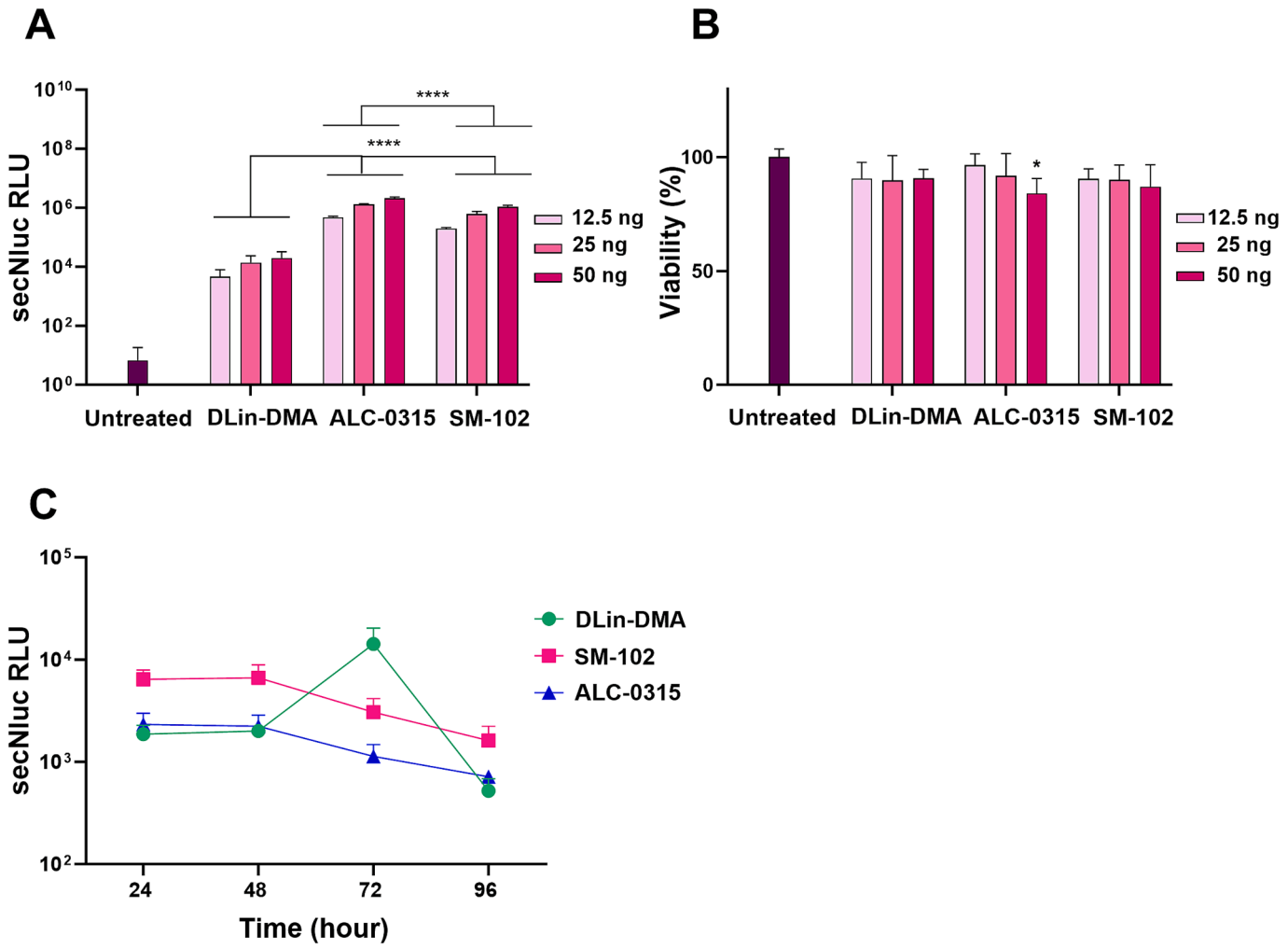

Fig. 4. Protein expression for iLCP formulations. (A) luciferase expression and (B) Cell viability for mRNA-loaded iLCPs formulated with DLin-DMA, SM-102, and ALC-0315 in MC3T3 cells after 24 h (n = 3). (C) Luminescence resulting from MC3T3 cells treated with iLCPs over a period of 96 h. Samples were obtained every 24 h for measurement of luciferase activity (n = 3). Data are shown as mean ± SD and $P < 0.05$ was considered statistically significant. All formulations were generated with mole fractions of lipids according to composition IV.

more efficiency for gene delivery compared to LNPs comprising other ionizable lipids (Ly et al., 2022; Maeki et al., 2023; Saraswat and Patel, 2023). All formulations fully preserved viability with only a slight reduction for ALC-0315-containing iLCP NPs at the highest concentration (Fig. 4B).

In the context of LNPs, key characteristics of ionizable lipids are the pKa of the protonatable group and the conical shape (Liu et al., 2021). A pKa of 6 to below 7 is required for high delivery efficiency and gives protonation only once the LNPs reach early endosomes (Carrasco et al., 2021; Sato et al., 2019). For DLin-DMA, SM-102, and ALC-0315 pKa values are 6.8, 6.68, and 6.09, respectively (Suzuki and Ishihara, 2021; Thi et al., 2021). The higher pKa value of SM-102 compared to ALC-0315 will lead to a greater positive charge at early stages of endosomal uptake.

ALC-0315 terminates in four acyl chains in comparison to three for SM-102. For maximal delivery, a cone shape is more desirable than a cylindrical shape as its incompatibility with the lipid bilayer leads to a destabilization of the endosomal membrane, triggering the release of nucleic acid payload into the cytosol (Carrasco et al., 2021; Liu et al., 2021). The higher activity of SM-102 in comparison to ALC-0315 indicates that for the iLCP NP the higher pKa benefitted delivery more.

Next, we addressed the kinetics of protein expression. MC3T3 cells were treated for 4 h with iLCP NPs and luciferase expression was assessed for up to 4 days. For SM-102 and ALC-0315 containing iLCP NPs the maximum level of protein expression was detected at ~ 48 h and then luciferase expression started declining. Interestingly, for DLin-DMA iLCP NPs expression peaked only at ~ 72 h (Fig. 4C). For all three iLCP NP formulations these kinetics point at a delayed release of the mRNA as for peptide and lipid micelle based formulations, maximum expression is already achieved after 24 h (van Asbeck et al., 2021).

3.5. *Physicochemical characterization of optimized iLCPs nanoparticles*

Following the successful development of delivery-competent iLCP NPs, we investigated in more detail the physicochemical characteristics of the formulations. The membrane-core structure is the prominent feature of LCP NPs that allows tuning of surface characteristics by using different lipid compositions in the outer layer. The individual lipids of the outer leaflet of the optimized iLCP NPs were ionizable lipids, DOTAP, cholesterol, and DSPE-PEG2000. For all three iLCP NPs, the same cores were used. In TEM images, the CaP cores exhibited well dispersed sphere-like particles with a diameter of ~ 25 nm and the typical hollow structure of CaP (Fig. 5A) (Li et al., 2012). The dispersity was preserved after coating with the lipid bilayer (Fig. 5B). However, because of the electron transparency of the lipid bilayer, only the CaP cores of LCP NPs were detected. Consistent with TEM, characterization of size by DLS gave a diameter of around 40 nm which was very similar for iLCP NPs with all three ionizable lipids (Fig. 5C). The zeta potentials

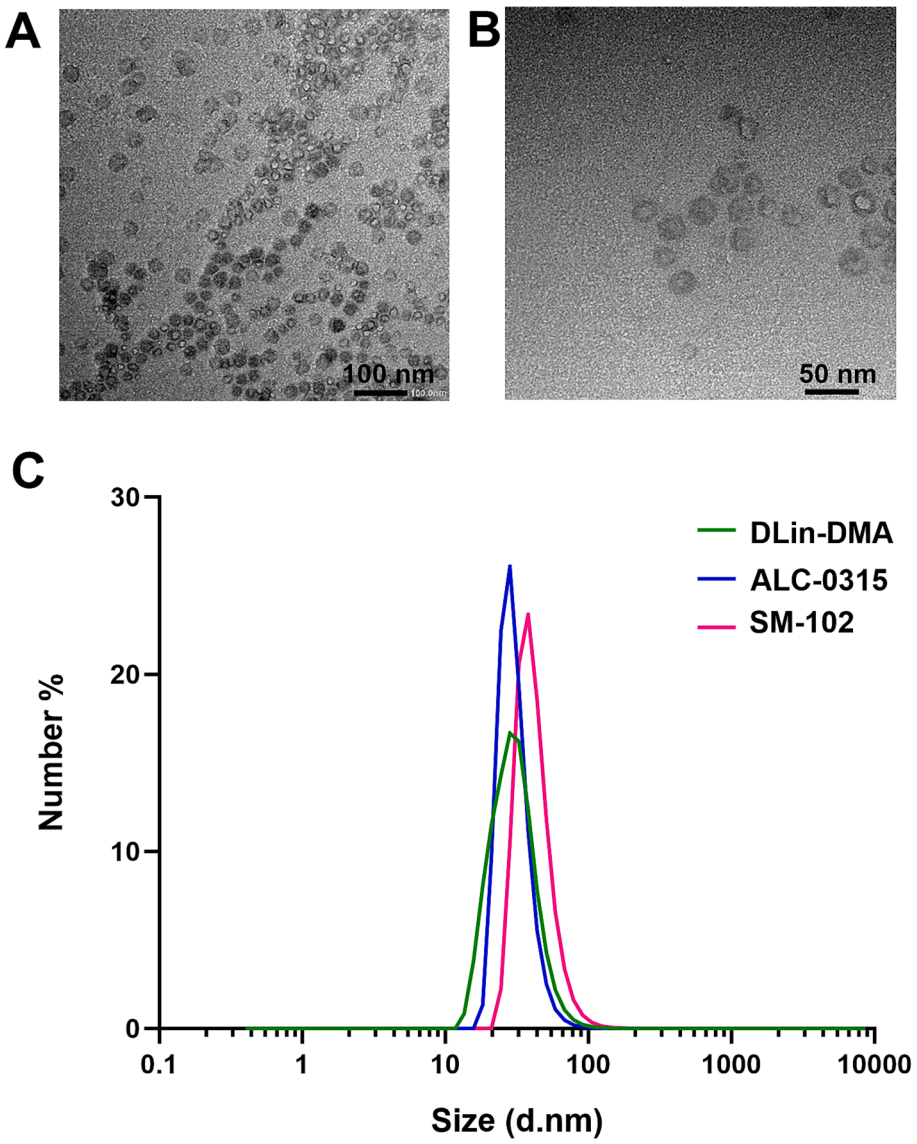

Fig. 5. Physicochemical characterization of iLCP NPs. (A) TEM images of CaP cores, and (B) of iLCPs. (C) Particle size distribution of iLCPs containing three different ionizable lipids. All iLCP NPs were formulated with lipid compositions according to formulation IV.

were between 20 and 28 mV (Table 3). With ~ 0.4 the polydispersity index (PDI) was rather high. Analysis of the DLS data by volume revealed a small aggregation peak in all formulations. However, when the size distribution was assessed by number, the peak was no longer visible (supplementary materials), indicating it did not constitute a significant fraction of overall particle population. Nevertheless, it could still contribute to an elevated PDI. The entrapment efficiency of mRNA was determined using QuantiFluor RNA System and it was around 46 % which is consistent with findings from previous studies on mRNA encapsulation in LCP NPs (Lin et al., 2022; Wang et al., 2018). According to the previous studies on LCP NPs, they are more efficient at encapsulating smaller oligonucleotides, such as siRNA, compared to larger molecules like mRNA (Huang et al., 2018; Lin et al., 2022).

Overall, the iLCP NPs were much smaller than common LNP formulations which have a diameter of about 75 to 90 nm (Zhang et al., 2023). Size governs tissue penetration and cellular uptake, thus it will be interesting to explore whether iLCP NPs show better tissue penetration than LNPs.

Table 3
Characterization of iLCP NPs. DLin-DMA stands for DLin-DMA. All iLCP were formulated with a composition of lipids according to formulation IV.

Sample	Hydrodynamic Diameter (nm)	Zeta potential (mv)	PDI
DLin-DMA iLCPs	31.2 ± 5.8	19.95 ± 0.7	0.43 ± 0.01
ALC-0315 iLCPs	30.7 ± 1.03	28.5 ± 0.3	0.47 ± 0.02
SM-102 iLCPs	42.3 ± 3.9	22.8 ± 1.1	0.42 ± 0.02

3.6. Cellular uptake of iLCP NPs

To better understand to which degree the ionizable lipids exerted their role in uptake and cytosolic delivery, cells were incubated with iLCP NP formulations incorporating fluorescently labeled mRNA. Next to LCP NP formulations incorporating ionizable lipids, also LCP NP formulations including only DOPC or DOTAP were included. Uptake efficiency fully correlated with transfection efficiency as observed for luciferase delivery (Fig. 6A, B). Both, DOPC and DOTAP LCP formulations showed only very little uptake. SM-102 iLCP NPs had the highest uptake, followed by ALC-0315 iLCP NP and DLin-DMA iLCP NPs. For

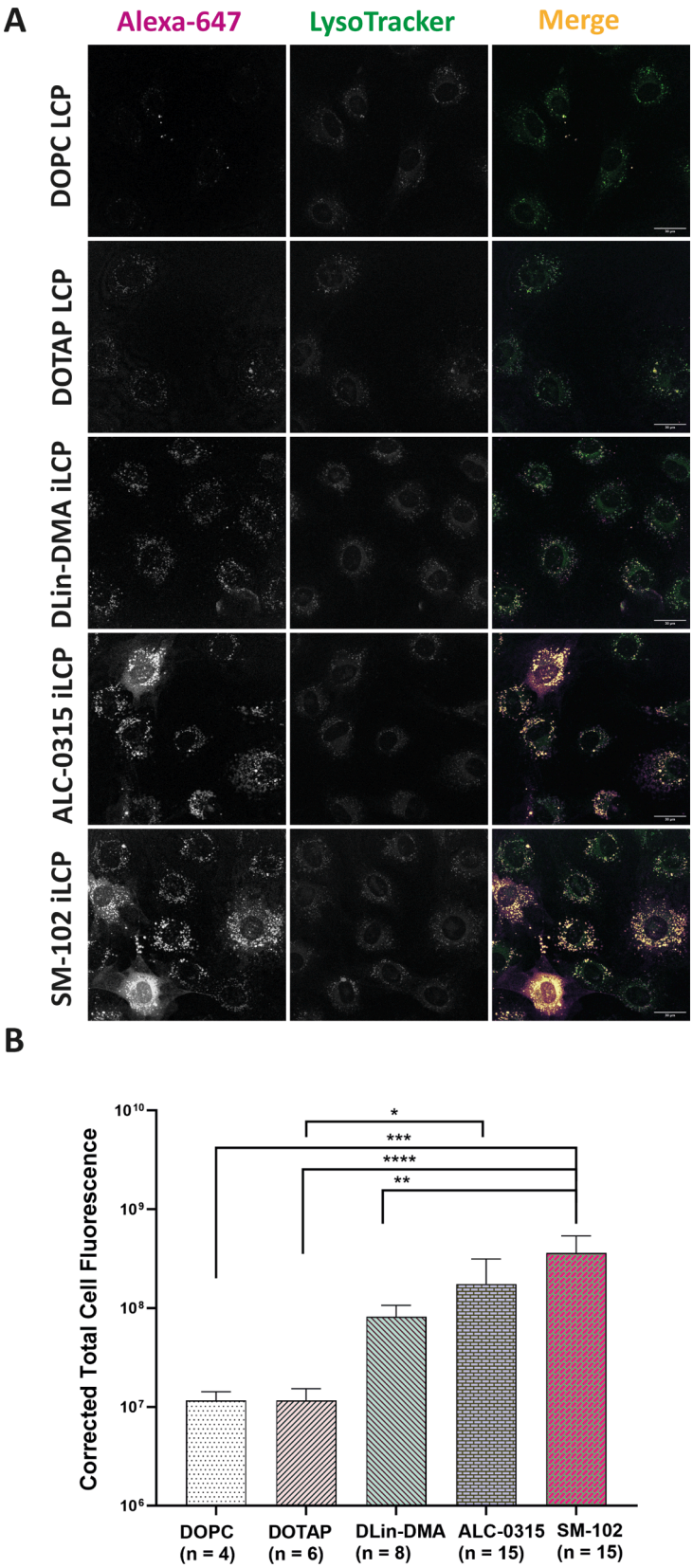

Fig. 6. Cellular uptake of iLCP NPs. (A) The subcellular distribution of iLCP NPs was imaged by confocal live cell microscopy in MC3T3 cells. Briefly, cultured cells were incubated with LCP NPs containing AlexaFluor647-labeled mRNA (50 μg) and 4 h post-transfection, cells were stained with LysoTracker (green) and images were captured. (B) Corrected total cell fluorescence of internalized Cy5-labeled mRNA was quantified from the images using ImageJ. All images were acquired using the same acquisition settings and are displayed with the same adjustments of contrast and brightness. The scale bar represents 30 μm. Data are shown as mean ± SD and $P < 0.05$ was considered statistically significant.

ALC-0315 and SM-102 homogenous fluorescence inside the nuclei provided evidence for cytosolic release of mRNA consistent with the high protein expression obtained by these formulations. The low internationalization of the formulation with the positively charged lipid DOTAP alone was unexpected as the positive charge should drive the interaction with the plasma membrane and induce cellular uptake (Albanese et al., 2012; Hald Albertsen et al., 2022). Thus, even though we expect only little protonation of the ionizable lipids outside cells they strongly contribute to cellular uptake.

4. Conclusion

In this study, we demonstrate that incorporation of an ionizable lipid into the outer lipid layer of LCP NPs greatly enhances cellular uptake and cytosolic delivery of mRNA. Cytotoxicity could be reduced effectively by also incorporating a pegylated lipid. In comparison to peptide and micelle-based formulations, the iLCP NPs showed a delayed expression kinetic which may be attributed to release of the mRNA from the calcium phosphate core. To our knowledge, this is the first study on optimization of LCP potency using ionizable lipids. Ionizable LCP NPs containing branched-tail lipids, SM-102 and ALC-0315, were more potent than DLin-DMA with only two unsaturated acyl chains. According to current concepts, in lipid NPs the ionizable lipid serves a dual purpose which is complexation of the oligonucleotide payload and destabilization of the endosomal membrane by assuming an inverted hexagonal phase due to the conical structure of the lipid. Here, we show that in iLCP NPs the ionizable lipid only exerts the second function independent from the first one as complexation occurs in the calcium phosphate core. This observation constitutes a new concept on the functionality of cone-shaped ionizable lipids in oligonucleotide formulations. It will be highly interesting to investigate in more detail the role of lipid shape and pKa of the head group to better understand to which degree the same or different rules apply as in LNP formulations. Furthermore, since the ionizable lipid is restricted to the outer layer of the nanoparticle, mRNA delivery with iLCP NPs is associated with a reduced load of non-endogenous lipids which may benefit biocompatibility, in particular for repeated applications (Jorgensen et al., 2023).

CRediT authorship contribution statement

Masoomeh Khalifeh: Writing – original draft, Methodology, Investigation, Formal analysis, Conceptualization. **Rik Oude Egberink:** Methodology, Investigation, Formal analysis. **Rona Roverts:** Methodology, Investigation, Formal analysis. **Roland Brock:** Writing – review & editing, Resources, Conceptualization.

Declaration of competing interest

The authors declare that they have no known competing financial interests or personal relationships that could have appeared to influence the work reported in this paper.

Acknowledgements

R.O.E. was supported by the Dutch Science Council (NWO TTW 17615), M. K. by Mashhad University of Medical Sciences Research Council, Mashhad, Iran.

Appendix A. Supplementary data

Supplementary data to this article can be found online at https://doi.org/10.1016/j.ijpharm.2024.125109.

Data availability

Data will be made available on request.

References

Albanese, A., Tang, P.S., Chan, W.C.W., 2012. The Effect of Nanoparticle Size, Shape, and Surface Chemistry on Biological Systems. Annu. Rev. Biomed. Eng. 14, 1–16. https://doi.org/10.1146/annurev-bioeng-071811-150124.

Benenato, K.E., Kumarasinghe, E.S., Cornebise, M., 2017. Compounds and compositions for intracellular delivery of therapeutic agents, in: WIPO/PCT (Ed.). Modernatx, USA.

Carrasco, M.J., Alishetty, S., Alameh, M.G., Said, H., Wright, L., Paige, M., Soliman, O., Weissman, D., Cleveland, T.E., Grishaev, A., Buschmann, M.D., 2021. Ionization and structural properties of mRNA lipid nanoparticles influence expression in intramuscular and intravascular administration. Commun Biol 4, 956. https://doi.org/10.1038/s42003-021-02441-2.

Dunbar, C.E., High, K.A., Joung, J.K., Kohn, D.B., Ozawa, K., Sadelain, M., 2018. Gene therapy comes of age. Science 359. https://doi.org/10.1126/science.aan4672.

Ezzat, K., Andaloussi, S.E., Zaghloul, E.M., Lehto, T., Lindberg, S., Moreno, P.M., Viola, J. R., Magdy, T., Abdo, R., Guterstam, P., Sillard, R., Hammond, S.M., Wood, M.J., Arzumanov, A.A., Gait, M.J., Smith, C.I., Hallbrink, M., Langel, U., 2011. PepFect 14, a novel cell-penetrating peptide for oligonucleotide delivery in solution and as solid formulation. Nucleic Acids Res. 39, 5284–5298. https://doi.org/10.1093/nar/gkr072.

Fröhlich, E., 2012. The role of surface charge in cellular uptake and cytotoxicity of medical nanoparticles. Int. J. Nanomed. 7, 5577–5591. https://doi.org/10.2147/ijn.S36111.

Hajj, K.A., Whitehead, K.A., 2017. Tools for translation: non-viral materials for therapeutic mRNA delivery. Nat. Rev. Mater. 2, 1–17.

Hald Albertsen, C., Kulkarni, J.A., Witzigmann, D., Lind, M., Petersson, K., Simonsen, J. B., 2022. The role of lipid components in lipid nanoparticles for vaccines and gene therapy. Adv. Drug Deliv. Rev. 188, 114416. https://doi.org/10.1016/j.addr.2022.114416.

Han, X., Zhang, H., Butowska, K., Swingle, K.L., Alameh, M.G., Weissman, D., Mitchell, M.J., 2021. An ionizable lipid toolbox for RNA delivery. Nat. Commun. 12, 7233. https://doi.org/10.1038/s41467-021-27493-0.

Hatakeyama, H., Ito, E., Akita, H., Oishi, M., Nagasaki, Y., Futaki, S., Harashima, H., 2009. A pH-sensitive fusogenic peptide facilitates endosomal escape and greatly enhances the gene silencing of siRNA-containing nanoparticles in vitro and in vivo. J. Control. Release 139, 127–132. https://doi.org/10.1016/j.jconrel.2009.06.008.

Hope, M.J., Mui, B.L., Lin, P.J., Barbosa, C.P., Madden, T.D., Ansell, S.M., Du, X., 2017. Lipid nanoparticle formulations, in: (PCT), W. (Ed.). Acuitas Therapeutics, USA.

Hou, X., Zaks, T., Langer, R., Dong, Y., 2021. Lipid nanoparticles for mRNA delivery. Nat. Rev. Mater. 6, 1078–1094. https://doi.org/10.1038/s41578-021-00358-0.

Huang, J.L., Chen, H.Z., Gao, X.L., 2018. Lipid-coated calcium phosphate nanoparticle and beyond: a versatile platform for drug delivery. J. Drug Target. 26, 398–406. https://doi.org/10.1080/1061186x.2017.1419360.

Jayaraman, M., Ansell, S.M., Mui, B.L., Tam, Y.K., Chen, J., Du, X., Butler, D., Eltepu, L., Matsuda, S., Narayanannair, J.K., Rajeev, K.G., Hafez, I.M., Akinc, A., Maier, M.A., Tracy, M.A., Cullis, P.R., Madden, T.D., Manoharan, M., Hope, M.J., 2012. Maximizing the potency of siRNA lipid nanoparticles for hepatic gene silencing in vivo. Angew. Chem. Int. Ed. Engl. 51, 8529–8533. https://doi.org/10.1002/anie.201203263.

Jorgensen, A.M., Wibel, R., Bernkop-Schnurch, A., 2023. Biodegradable Cationic and Ionizable Cationic Lipids: A Roadmap for Safer Pharmaceutical Excipients. Small 19, e2206968. https://doi.org/10.1002/smll.202206968.

Lechanteur, A., Furst, T., Evrard, B., Delvenne, P., Hubert, P., Piel, G., 2016. PEGylation of lipoplexes: The right balance between cytotoxicity and siRNA effectiveness. Eur. J. Pharm. Sci. 93, 493–503. https://doi.org/10.1016/j.ejps.2016.08.058.

Li, J., Chen, Y.C., Tseng, Y.C., Mozumdar, S., Huang, L., 2010. Biodegradable calcium phosphate nanoparticle with lipid coating for systemic siRNA delivery. J. Control. Release 142, 416–421. https://doi.org/10.1016/j.jconrel.2009.11.008.

Li, S., Hu, Y., Li, A., Lin, J., Hsieh, K., Schneiderman, Z., Zhang, P., Zhu, Y., Qiu, C., Kokkoli, E., Wang, T.H., Mao, H.Q., 2022. Payload distribution and capacity of mRNA lipid nanoparticles. Nat. Commun. 13, 5561. https://doi.org/10.1038/s41467-022-33157-4.

Li, J., Yang, Y., Huang, L., 2012. Calcium phosphate nanoparticles with an asymmetric lipid bilayer coating for siRNA delivery to the tumor. J. Control. Release 158, 108–114. https://doi.org/10.1016/j.jconrel.2011.10.020.

Lin, X., Chen, H., Xie, Y., Zhou, X., Wang, Y., Zhou, J., Long, S., Hu, Z., Zhang, S., Qiu, W., Zeng, Z., Liu, L., 2022. Combination of CTLA-4 blockade with MUC1 mRNA nanovaccine induces enhanced anti-tumor CTL activity by modulating tumor microenvironment of triple negative breast cancer. Transl. Oncol. 15, 101298. https://doi.org/10.1016/j.tranon.2021.101298.

Liu, S., Cheng, Q., Wei, T., Yu, X., Johnson, L.T., Farbiak, L., Siegwart, D.J., 2021. Membrane-destabilizing ionizable phospholipids for organ-selective mRNA delivery and CRISPR–Cas gene editing. Nat. Mater. 20, 701–710. https://doi.org/10.1038/s41563-020-00886-0.

Ly, H.H., Daniel, S., Soriano, S.K.V., Kis, Z., Blakney, A.K., 2022. Optimization of Lipid Nanoparticles for saRNA Expression and Cellular Activation Using a Design-of-Experiment Approach. Mol. Pharm. 19, 1892–1905. https://doi.org/10.1021/acs.molpharmaceut.2c00032.

Maeki, M., Okada, Y., Uno, S., Sugiura, K., Suzuki, Y., Okuda, K., Sato, Y., Ando, M., Yamazaki, H., Takeuchi, M., Ishida, A., Tani, H., Harashima, H., Tokeshi, M., 2023. Mass production system for RNA-loaded lipid nanoparticles using piling up microfluidic devices. Appl. Mater. Today 31, 101754. https://doi.org/10.1016/j.apmt.2023.101754.

Movahedi, F., Gu, W., Soares, C.P., Xu, Z.P., 2021. Encapsulating anti-parasite benzimidazole drugs into lipid-coated calcium phosphate nanoparticles to efficiently induce skin cancer cell apoptosis. Front. Nanotechnol. 3, 693837.
Oude Egberink, R., van Schie, D.M., Joosten, B., de Muynck, L.T.A., Jacobs, W., van Oostrum, J., Brock, R., 2024. Unraveling mRNA delivery bottlenecks of ineffective delivery vectors by co-transfection with effective carriers. Eur J Pharm Biopharm, 114414. https://doi.org/10.1016/j.ejpb.2024.114414.
Paloncýová, M., Čechová, P., Šrejber, M., Kührová, P., Otyepka, M., 2021. Role of Ionizable Lipids in SARS-CoV-2 Vaccines As Revealed by Molecular Dynamics Simulations: From Membrane Structure to Interaction with mRNA Fragments. J. Phys. Chem. Lett. 12, 11199–11205. https://doi.org/10.1021/acs.jpclett.1c03109.
Pardi, N., Hogan, M.J., Porter, F.W., Weissman, D., 2018. mRNA vaccines - a new era in vaccinology. Nat. Rev. Drug Discov. 17, 261–279. https://doi.org/10.1038/nrd.2017.243.
Rabanel, J.M., Hildgen, P., Banquy, X., 2014. Assessment of PEG on polymeric particles surface, a key step in drug carrier translation. J. Control. Release 185, 71–87. https://doi.org/10.1016/j.jconrel.2014.04.017.
Ramezanpour, M., Tieleman, D.P., 2022. Computational Insights into the Role of Cholesterol in Inverted Hexagonal Phase Stabilization and Endosomal Drug Release. Langmuir 38, 7462–7471. https://doi.org/10.1021/acs.langmuir.2c00430.
Sahin, U., Karikó, K., Türeci, Ö., 2014. mRNA-based therapeutics–developing a new class of drugs. Nat. Rev. Drug Discov. 13, 759–780. https://doi.org/10.1038/nrd4278.
Saraswat, A., Patel, K., 2023. Delineating effect of cationic head group and preparation method on transfection versus toxicity of lipid-based nanoparticles for gene delivery.
Sato, Y., Hashiba, K., Sasaki, K., Maeki, M., Tokeshi, M., Harashima, H., 2019. Understanding structure-activity relationships of pH-sensitive cationic lipids facilitates the rational identification of promising lipid nanoparticles for delivering siRNAs in vivo. J. Control. Release 295, 140–152. https://doi.org/10.1016/j.jconrel.2019.01.001.
Satterlee, A.B., Yuan, H., Huang, L., 2015. A radio-theranostic nanoparticle with high specific drug loading for cancer therapy and imaging. J. Control. Release 217, 170–182. https://doi.org/10.1016/j.jconrel.2015.08.048.
Schlich, M., Palomba, R., Costabile, G., Mizrahy, S., Pannuzzo, M., Peer, D., Decuzzi, P., 2021. Cytosolic delivery of nucleic acids: The case of ionizable lipid nanoparticles. Bioeng. Transl. Med. 6, e10213. https://doi.org/10.1002/btm2.10213.
Shang, L., Nienhaus, K., Nienhaus, G.U., 2014. Engineered nanoparticles interacting with cells: size matters. J Nanobiotechnology 12, 1–11. https://doi.org/10.1186/1477-3155-12-5.
Suzuki, Y., Ishihara, H., 2021. Difference in the lipid nanoparticle technology employed in three approved siRNA (Patisiran) and mRNA (COVID-19 vaccine) drugs. Drug Metab. Pharmacokinet. 41, 100424. https://doi.org/10.1016/j.dmpk.2021.100424.
Tang, J., Li, L., Howard, C.B., Mahler, S.M., Huang, L., Xu, Z.P., 2015. Preparation of optimized lipid-coated calcium phosphate nanoparticles for enhanced in vitro gene delivery to breast cancer cells. J. Mater. Chem. B 3, 6805–6812. https://doi.org/10.1039/c5tb00912j.
Thi, T.T.H., Suys, E.J.A., Lee, J.S., Nguyen, D.H., Park, K.D., Truong, N.P., 2021. Lipid-Based Nanoparticles in the Clinic and Clinical Trials: From Cancer Nanomedicine to COVID-19 Vaccines. Vaccines 9, 359.
van Asbeck, A.H., Dieker, J., Oude Egberink, R., van den Berg, L., van der Vlag, J., Brock, R., 2021. Protein Expression Correlates Linearly with mRNA Dose over Up to Five Orders of Magnitude In Vitro and In Vivo. Biomedicines 9, 511. https://doi.org/10.3390/biomedicines9050511.
Vermeulen, L.M.P., De Smedt, S.C., Remaut, K., Braeckmans, K., 2018. The proton sponge hypothesis: Fable or fact? Eur. J. Pharm. Biopharm. 129, 184–190. https://doi.org/10.1016/j.ejpb.2018.05.034.
Wang, Y., Zhang, L., Xu, Z., Miao, L., Huang, L., 2018. mRNA Vaccine with Antigen-Specific Checkpoint Blockade Induces an Enhanced Immune Response against Established Melanoma. Mol. Ther. 26, 420–434. https://doi.org/10.1016/j.ymthe.2017.11.009.
Yang, Y., Li, J., Liu, F., Huang, L., 2012. Systemic delivery of siRNA via LCP nanoparticle efficiently inhibits lung metastasis. Mol. Ther. 20, 609–615. https://doi.org/10.1038/mt.2011.270.
Yu, B., Wang, X., Zhou, C., Teng, L., Ren, W., Yang, Z., Shih, C.-H., Wang, T., Lee, R.J., Tang, S., Lee, L.J., 2014. Insight into Mechanisms of Cellular Uptake of Lipid Nanoparticles and Intracellular Release of Small RNAs. Pharm. Res. 31, 2685–2695. https://doi.org/10.1007/s11095-014-1366-7.
Zhang, L., More, K.R., Ojha, A., Jackson, C.B., Quinlan, B.D., Li, H., He, W., Farzan, M., Pardi, N., Choe, H., 2023. Effect of mRNA-LNP components of two globally-marketed COVID-19 vaccines on efficacy and stability. npj Vaccines 8, 156. https://doi.org/10.1038/s41541-023-00751-6.
Zuhorn, I.S., Bakowsky, U., Polushkin, E., Visser, W.H., Stuart, M.C., Engberts, J.B., Hoekstra, D., 2005. Nonbilayer phase of lipoplex-membrane mixture determines endosomal escape of genetic cargo and transfection efficiency. Mol. Ther. 11, 801–810. https://doi.org/10.1016/j.ymthe.2004.12.018.